Below bandgap CW laser modification of ZnO:Al thin film with Ag nanoparticles

Maksim M. Sergeev, Vladislav R. Gresko, Yaroslava M. Andreeva, Lilia A. Sokura, Elena V. Shirshneva-Vaschenko, Tatiana E. Itina, Georgy V. Varigyn

Below bandgap CW laser modification of ZnO:Al thin film with Ag nanoparticles

Maksim M. Sergeev[a], Vladislav R. Gresko[a*], Yaroslava M. Andreeva[a], Lilia A. Sokura[b], Elena V. Shirshneva-Vaschenko[c], Tatiana E. Itina[d], Georgy V. Varigyn[e]

[a] Faculty of Laser Photonics and Optoelectronics, ITMO University, 197101 St. Petersburg, Russia
[b] Institute of Advanced Data Transfer Systems, ITMO University, 197101 St. Petersburg, Russia
[c] College of Optics and Photonics, CREOL, University of Central Florida 4304 Scorpius Street, Orlando, Florida 32816, USA
[d] Laboratoire Hubert Curien, UMR CNRS 5516/UJM/Univ. Lyon, Bat. F, 18 rue du Pr. Benoit Lauras, 42000 Saint-Etienne, France
[e] St. Petersburg State University, 7/9 Universitetskaya nab, St. Petersburg, Russia 199034
* Correspondence author: gresko.97@mail.ru.

Abstract:

The paper presents a CW laser modification of ZnO:Al thin films with silver nanoparticles. When exposed to radiation with power densities I_0 = 0.89 MW/cm^2 and I_0 = 1.07 MW/cm^2 and scanning velocities V_{sc} = 100 μm/s and V_{sc} = 50 μm/s, the film structure became denser, the size of ZnO:Al crystallites increased, and the size of silver nanoparticles decreased. The effect of radiation on the optical characteristics of the samples was investigated. Blue shift of the plasmon resonance peak and an increase in the bandgap from 3.27 eV to 3.36 eV were obtained. A photothermal film processing mechanism was proposed.

Keywords: sol-gel composites; ZnO:Al thin films; laser influence; plasmon resonance; Ag nanoparticles; phase transformation

1. Introduction

ZnO:Al (AZO) thin films are widely used in optoelectronics as transparent electrodes [1], in solar cells as active or window layers [2], and as photodetectors of UV radiation [3]. Laser structural modification of such AZO thin films is a quite novel technological solution. It has already been successfully implemented using pulsed radiation from an excimer KrF laser with a wavelength of λ = 248 nm [4–6]. The radiation source was chosen primarily due to the high spectral absorption of AZO films in the UV spectral region, where the intrinsic absorption of the matrix starts at λ < 370 nm [5]. Since 1997 it has been shown that optical and electrical characteristics of AZO films can change due to local thermal action of laser radiation on the matrix [5], resulting in its sintering [4] and recrystallization [7–9]. Laser influence in the optimal regime can lead to a decrease in electrical resistance, an increase in the mobility of electrons and a decrease in their concentration in the modified areas. In this case, optical transmission in the visible range decreases

by 10% in the modified areas, the transmission in the IR range increases, and the bandgap energy decreases[4].

However, the use of excimer lasers has revealed several drawbacks that significantly limit the applicability of laser methods for semiconductor thin films processing. First, the laser radiation wavelength in the deep UV range and the short pulse duration (4-10 ns) lead to the accumulation of excessive absorbed energy in the film. This may be a reason for AZO thin films destruction due to high tension. Second, the low repetition rate of excimer laser pulses results in the inability to use it together with scanning systems. Therefore, these factors narrow the area of optimal processing conditions. On the other hand, the complexity of an excimer laser operation, specific optics for beam focusing and the risk of human skin deep UV exposure significantly limit the use of excimer lasers in industry.

Recently, new functional photonic materials with incorporation of Ag, Au, and Cu nanoparticles (NPs) have been developed to activate the effects of localized plasmon resonance [10,11], while the materials with Fe and Co NPs activate ferroelectric effects [12]. This strategy is used to increase the efficiency of photovoltaics [13], photocatalysis [14] and photodetection [15] devices. In this case, the absorption of the composite film with NPs increases in the near UV and visible spectral regions. This allows to abandon the radiation of excimer lasers and switch to commonly available semiconductor lasers with continuous wave (CW) radiation on wavelengths from 380 to 450 nm in violet (V) spectral range and the radiation power from 0.2 to 3.0 W in the focused beam processing mode. The proposed method significantly simplifies thin films processing, allows the use of commercially available laser sources and optical elements. In addition, this reduces safety requirements for laser systems.

The research aims to investigate local changes in properties of AZO semiconductor thin films with Ag NPs under “soft” CWV laser irradiation. The morphological and spectral characteristics of films before and after laser exposure were studied and a mechanism of film laser treatment was proposed.

2. Materials and Methods

Thin polycrystalline AZO thin films with Ag NPs (AZO:Ag) were obtained by the sol-gel method [16]. The AZO films were created from the solution of zinc acetate and aluminum nitrate in ethylene glycol monomethyl ether with a concentration of 0.2 M. The percentage of Al in the films was 0.5 wt%. An AZO film was deposited onto a 1 mm thick fused silica substrate by centrifugation. To achieve film thickness h = 120 ± 5 nm the deposition of layers was repeated 10 times. After each deposition the sample was dried at 300°C for 5 minutes to evaporate the solvent. To obtain Ag NPs, a solution of silver nitrate in ethylene glycol monomethyl ether with a

concentration of 0.03 M was created. A layer of Ag NPs inside the AZO film was obtained by sequential deposition of 5 layers of AZO and silver solutions.

Since the initial grain size in the film was only 3-5 nm, the final stage of obtaining a polycrystalline AZO film with Ag NPs was the stage of heat treatment (HT) of the layers in the muffle furnace. HT was performed in air at a temperature of 570°C for 15 minutes and provided crystallization and coarsening of AZO grains and Ag NPs to a size of 15-25 nm. Processing in the furnace did not lead to significant changes in h, which varied within the error. In turn, Ag atoms/ions were migrating through the thickness of the AZO matrix forming Ag NPs in the initial layer.

The semiconductor CWV laser LSR405CP-2W with λ = 405 nm was used for film processing (Fig. 1). The initial TEM_{10} beam after the diaphragm had a square cross section of 1.5x1.5 mm and uniform intensity distribution. Laser radiation was focused by a 60x objective (NA = 0.85) with focal length F = 200 μm into the beam with radius r_0 = 1.5 μm. A three-coordinate movable table provided scanning over the sample surface. During the tracks recording the incident power on the film equaled P = 20 mW and P = 24 mW, which corresponded to the power density I_0 = 0.89 MW/cm^2 and I_0 = 1.07 MW/cm^2. The scanning velocity during the recording tracks was V_{sc} = 100 μm/s and V_{sc} = 50 μm/s.

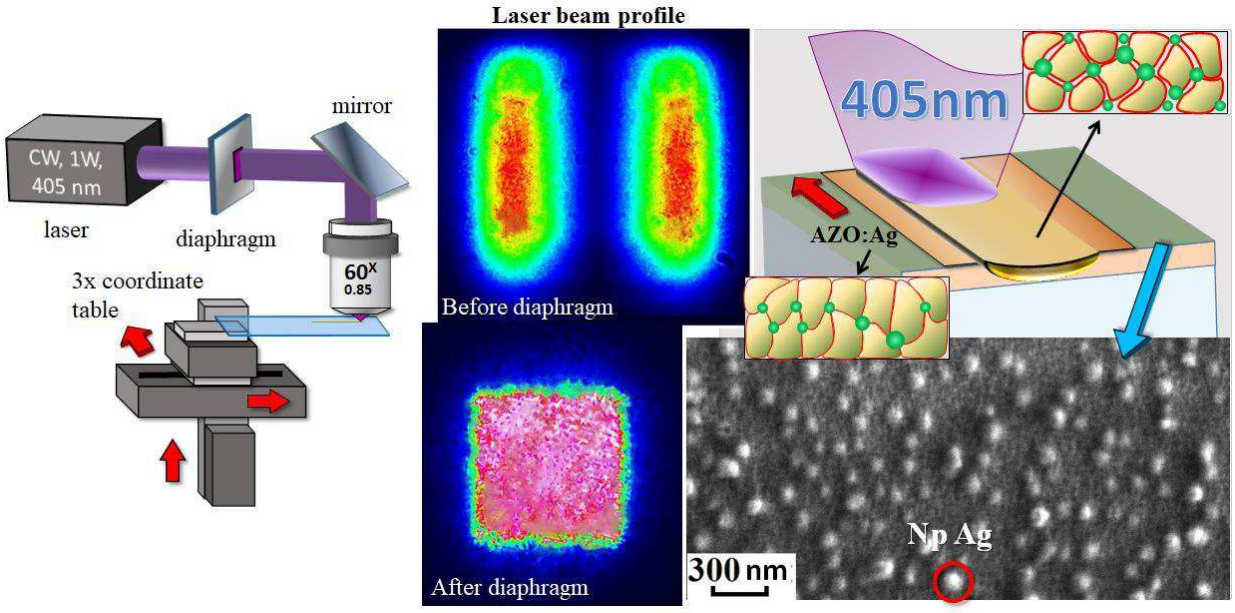

Fig. 1. (a) Experimental setup scheme for laser modification of AZO: Ag thin films in the matrix crystallization regime with growth / decomposition of Ag NPs; (b) original film SEM image.

After laser exposure, the sample surface was studied using an optical microscope, Carl Zeiss Axio Imager A1M in the reflected and transmitted light, in the bright and dark field. The

morphology of the film relief was studied using a scanning probe microscope (SPM) NANOEDUCATOR and a scanning electron microscope (SEM). Spectral characteristics of the films in the spectral range from 200 nm to 1100 nm were studied using the SF-56 spectrophotometer. The optical characteristics of the treated areas were investigated in the spectral range from 330 nm to 800 nm using a microscope-spectrophotometer MSFU-K with a photometric area of 2.5 μm.

3. Results and Discussion

3.1 Optical constants of initial material

Spectral transmission (T_{meas}) and reflection (R_{meas}) of non-polarized light at normal incidence were measured (Fig. 2). T_{meas} spectra of AZO:Ag shows the plasmon resonance peak with a minimum near 475 nm (green curve), which after HT shifted to 610 nm (orange curve). This peak is distinctive for Ag NPs, their size increased after HT. The 355 nm peak is distinctive for samples after HT in the furnace. This peak is located at the edge of the AZO matrix fundamental absorption. It indicates the incorporation of Al atoms into the ZnO matrix and the formation of the corresponding crystals [17,18], which leads to a decrease in the bandgap [19]. In R_{meas} spectra there is a similar plasmon peak near 487 nm, which shifted to 790 nm after HT. The HT of AZO:Ag films led to a decrease in transmission and an increase in reflection, that indirectly indicates metallization due to the formation and coarsening of Ag NPs, as well as compaction of the matrix itself. Another notable peak near 1030 nm is distinctive for all samples in both the transmission and reflection spectra.

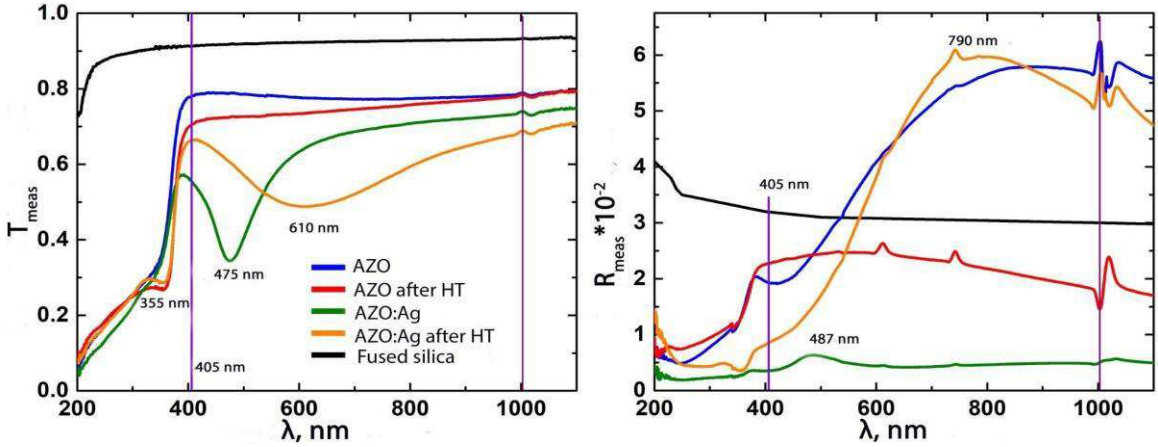

Fig. 2. Transmission and reflection of AZO films without HT (blue curve) and after HT in the furnace (red curve), as well as AZO:Ag without HT (green curve) and after HT in the furnace (orange curve).

Optical constants of the films were calculated using numerical method [20]. The extinction k_f was calculated according to the spectral characteristics of T_{meas} and R_{meas} (Fig. 3). Calculation error was high in the spectral range 200 - 350 nm, which is characteristic of low transmission in the region of fundamental absorption of the film matrix.

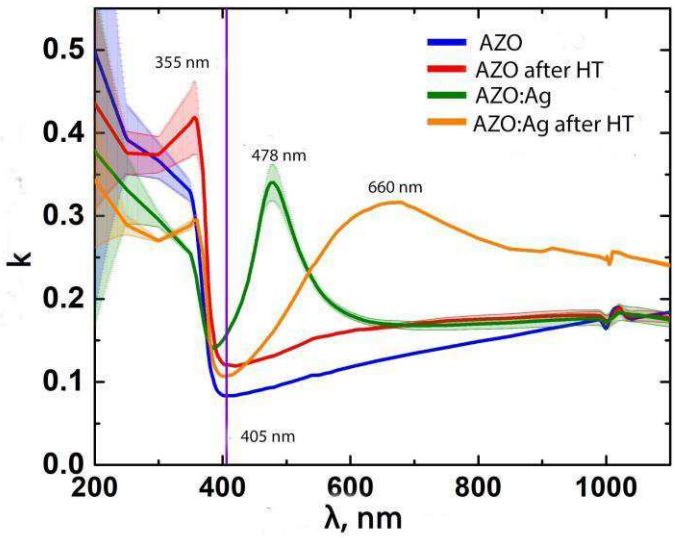

Fig. 3. Extinction of AZO and AZO: Ag films without HT and after HT in the furnace.

The k_f curves clearly show that the HT stage did not lead to a significant change in the extinction of the AZO matrix (Fig. 3). The addition of silver to AZO/Ag films led to an abrupt increase in extinction near 478 nm before HT. After HT its value increased significantly in the spectral range of 500 - 1100 nm. This indicates an increase in the volume fraction of the second phase in the form of Ag NPs after HT.

The bandgap energy E_g in the AZO and AZO:Ag systems was determined using relation $\alpha h\nu = B(h\nu - E_g)^{\gamma}$ [21], where $\alpha = 2\pi k_f(\lambda)/\lambda$ is the absorption index; $h\nu$ is the energy of the incident photons; B is a constant that depends on the concentration and mobility of free charge carriers in the material and denotes the length of the bandgap; γ is the gain for all possible transitions in the electronic system. The coefficient γ corresponds to 1/2 for direct allowed, 3/2 for direct forbidden, 2 for indirect allowed and 3 for indirect forbidden transitions [22]. Usually, $\gamma = 1/2$ is typical for crystalline solids and $\gamma = 2$ for amorphous materials. Based on the k_f data, the corresponding dependences were plotted (Fig. 4). The energy of direct allowed transitions ($\gamma = 1/2$) was: 1.9 eV for AZO, 1.55 eV for AZO after HT, 1.22 eV for AZO:Ag, and 1.45 eV for AZO:Ag after HT. The presence of Ag in the film led to a decrease in the transition energy. However, after HT in the furnace, transition energy increased again. The energy of indirect allowed transitions ($\gamma = 2$) increased to the following values: 3.29 eV for AZO, 3.26 eV for AZO after HT in the furnace, 3.25 eV for AZO:Ag, and 3.27 eV for AZO:Ag after HT.

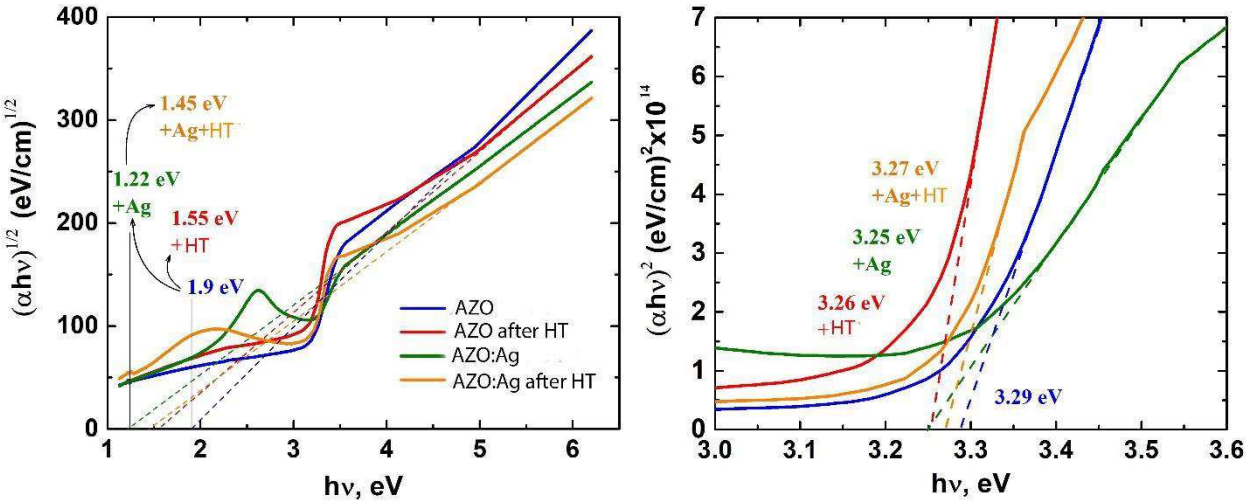

Fig. 4. Dependences $(\alpha h\nu)^{1/2}$ (right) and $(\alpha h\nu)^2$ (left) on the photon energy of incident radiation *hν* for AZO and AZO:Ag films.

3.2 Laser treatment

For laser treatment, AZO:Ag samples after HT were used. The wavelength of laser radiation (405 nm) lies at the edge of the fundamental absorption of the AZO matrix. And weakly absorbs by such films without NPs. The addition of Ag to the AZO film stage led to an increase in absorption from 0.20 to 0.44. After HT in the furnace, the presence of Ag NPs in the film changed the absorption from 0.28 to 0.35. Thus, the HT led to an increase in absorption by 0.11 with Ag NPs and by 0.08 without them. The absorption by NPs made it possible to reduce the intensity of the incident radiation. Moreover, the photothermal process of film modification was activated because the film was additionally heated by NPs, which absorb laser radiation. As a result of laser treatment, the morphological properties of the film were modified. The study of the sample relief using the SPM showed that the relief shrank by 20 - 50 nm after laser treatment. (Fig. 5).

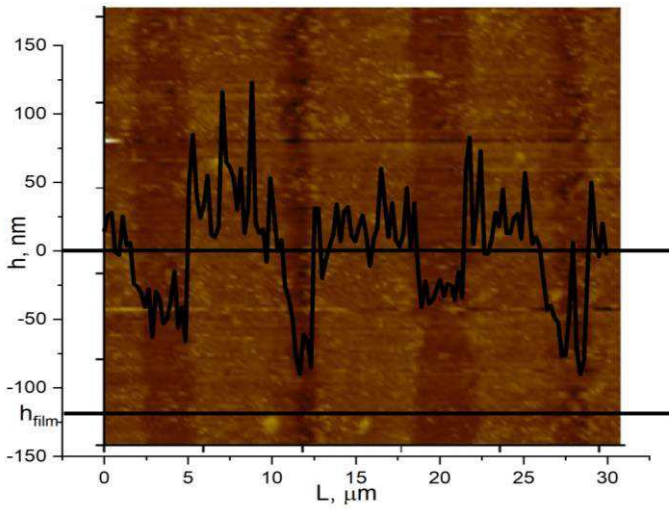

Fig. 5. a) 2D image (top view) of the tracks relief obtained with the SPM, b) A-A section.

In the SEM image the modified regions are darker than the original film, which indicates an increase in the film density (Fig. 6 a). The results of optical microscopy show the change in optical characteristics after laser treatment. From the optical image in the transmitted light mode one can see the brightening of the film in the irradiated area (fig. 6b), while darkening is observed in the reflected light mode (Fig. 6d). The dark field image shows that the tracks recorded at 0.89 MW/cm^2 were optically brighter (Fig. 6 c), that means they scattered the radiation more strongly and had greater roughness. SEM data also show that the AZO matrix was heated to the softening temperature with the activation of viscous flow along the track. A high speed of heating and cooling led to the formation of cavitation pores, as well as to the decomposition of large NPs into smaller ones (Fig. 6).

Additionally, the film was studied by SEM with a higher accelerating voltage (Fig. 7). The film had a polycrystalline structure and consisted of AZO grains about 20 nm in size, separated by dark voids and amorphous material 10 nm size. The figure also shows a histogram of the Ag NPs distribution by diameter over the area of 1.5x1.5 μm^2. As a first approximation, it was assumed that all NPs are spherical. The diameter of Ag NPs varied from 50 to 100 nm. Most NPs had a diameter of about 65 nm.

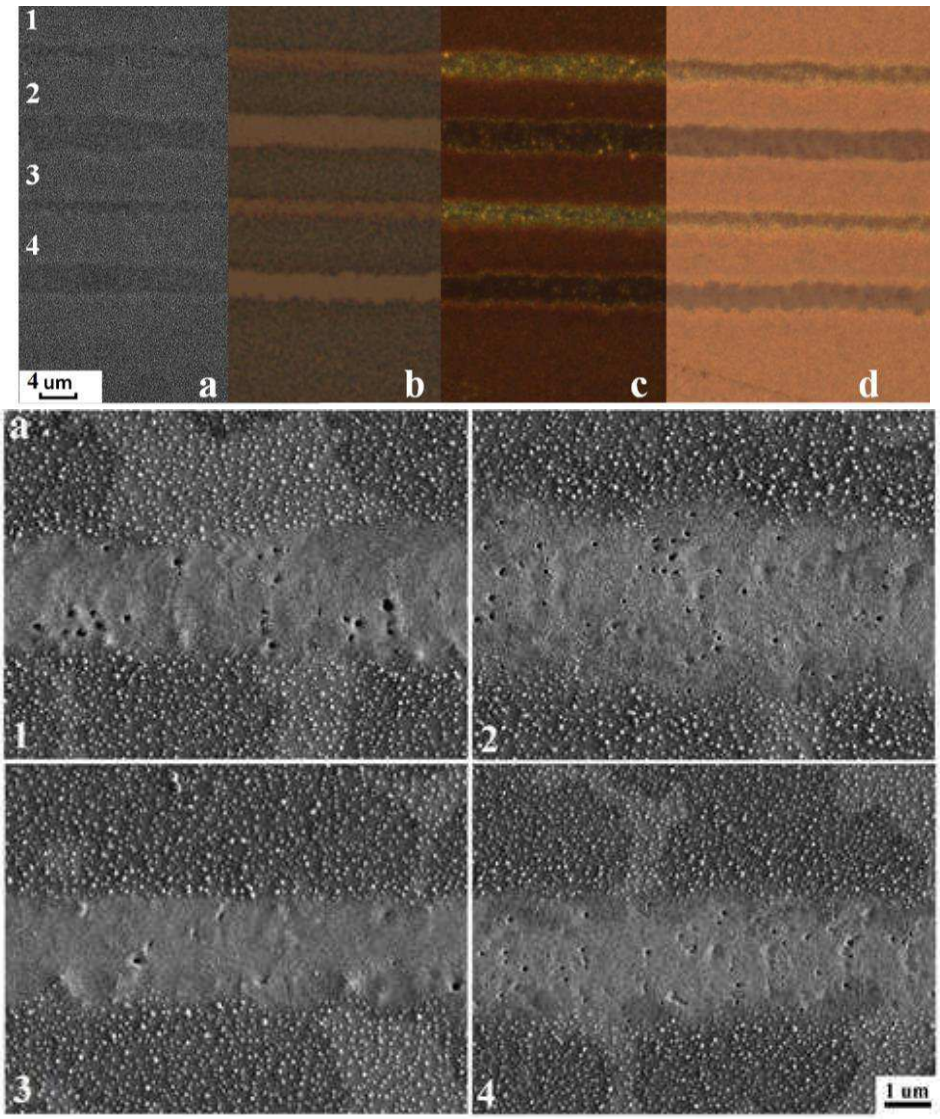

Fig. 6. (a) SEM images 1 – 50 μm/s, 0.89 MW/cm^2; 2 – 50 μm/s, 1.07 MW/cm^2; 3 – 100 μm/s, 0.89 MW/cm^2; 4 – 100 μm/s, 1.07 MW/cm^2; optical images in (b) transmitted light of bright field, (c) reflected light of dark field, (d) reflected light of bright field of the recorded track.

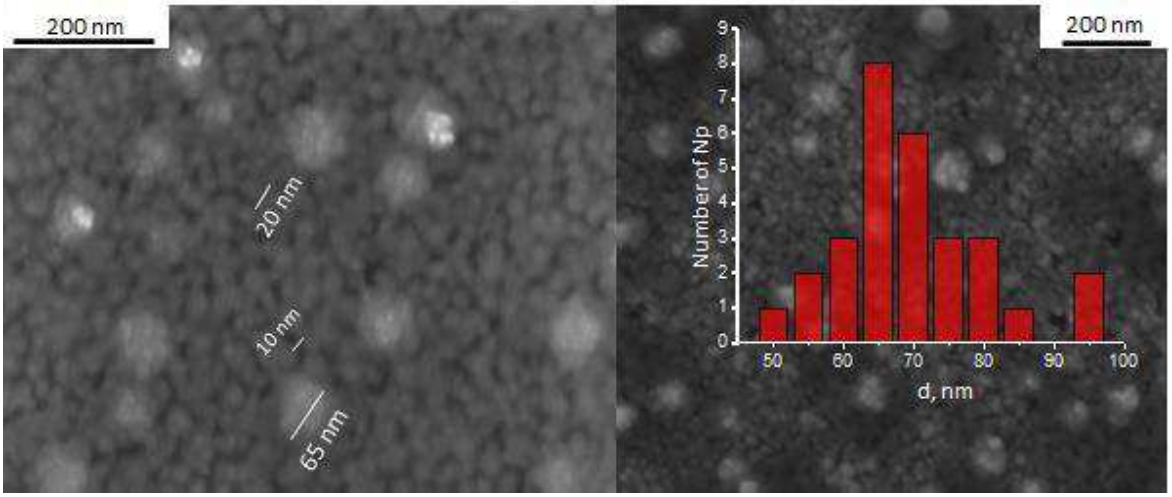

Fig. 7. SEM images of the original film and a histogram of Ag NPs size distribution by diametral size.

SEM images are shown in Fig. 8. The result of laser treatment is similar to the pulsed laser recrystallization with excimer laser [4]. Recrystallization of such films occurs when a certain temperature (Tcr) is reached. According to [4], the temperatures required for this process should be higher than 75% of the melting point (Tm). For AZO without NPs, Tm ≈ 1400 K, hence Tcr ≈ 1050 K (777 °C). Under the laser radiation thermal energy increases, individual grains melt and combine into crystallites with the following rapid solidification. In this experiment recrystallization was achieved due to the presence of Ag NPs in the film, they increased the absorption of laser radiation. After laser treatment NPs were distributed within crystallites, missing between them. The small dark voids in the original film disappeared after laser treatment. The diameter of the formed crystallites varied from 20 to 120 nm.

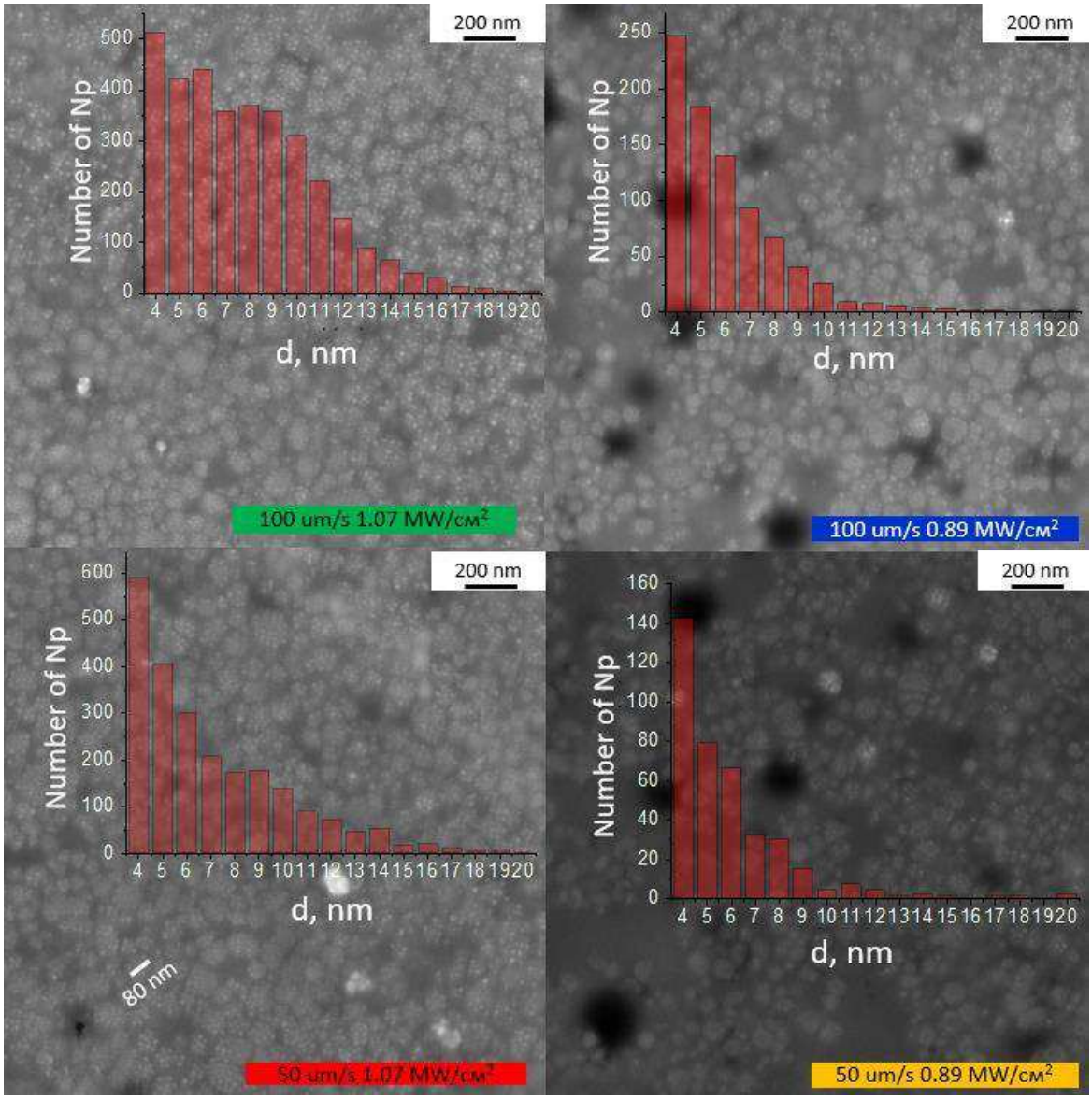

Fig. 8. SEM images of tracks. Non-crystallized areas are marked with a red circle. The color marks in the figures correspond to the colors of the spectral curves in Fig. 9. Red cycle corresponds to non-crystallized regions.

Fig. 8 shows histograms of NPs size distribution inside the tracks. For all regimes, the sizes of NPs remain the same, about 10 nm diameter or less. The highest concentration of NPs of all sizes in the track section 1.5x1.5 μm^2 was observed at 1.07 MW/cm^2: 3400 and 2250 for 100 μm/s and 50 μm/s, respectively. The concentrations for 0.89 MW/cm^2 were 400 and 800 for 100 μm/s and 50 μm/s, respectively. At the same time, in the tracks recorded at 0.89 MW/cm^2, large non-crystallized regions without NPs were observed. The proportion of such regions in the track area was 0.18 and 0.22 for 100 μm/s and 50 μm/s, respectively. The boundary between the original film and the recrystallized area was quite sharp (fig. 9).

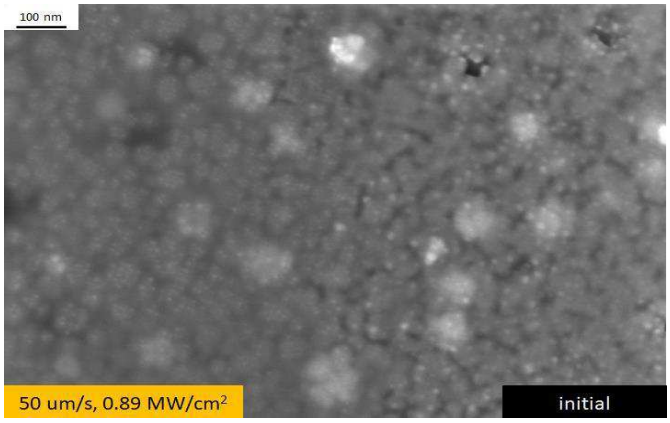

Fig. 9. SEM image of the area at the border of the track and the original film.

T_{meas} and R_{meas} spectra are shown in Fig. 10. T_{meas} curves at 0.89 MW/cm^2 (blue and orange curves) are similar to the spectra of the AZO:Ag films without HT (Fig. 2 a, green curve) due to plasmon peaks near the UV region. The intensity of the peak minimum in the transmission spectra are less than for the initial film: 0.39 for the initial AZO:Ag (dark curve), 0.52 and 0.57 at 100 μm/s and 50 μm/s, respectively. An increase in the radiation intensity to 1.07 MW/cm^2 led to a reverse shift of the plasmon resonance peaks to the IR region, with the minimum near 0.7. Decrease in the scanning velocity from 100 to 50 μm/s led to a shift in the minimum of transmission spectra to IR by 22–25 nm, irrespective of the radiation intensity. For both regimes the brightening of the film occurred. Its transmission after processing increased (Fig. 10). The highest transmission was obtained at 100 μm/s and 1.07 MW/cm^2.

For the reflection spectra there were also peaks with a maximum near 650-660 nm. Moreover, the intensity of these peaks, as well as the average reflection for the treated areas, was lower than that of the original film. An increase in transmission and a decrease in reflection attributed to a decrease in the film thickness. In addition, the recrystallization of the film caused these changes through reducing the number of defects in the AZO structure. In the polycrystalline film they were additional centers of scattering and absorption of radiation. A decrease in the

concentration of NPs can lead to similar effects. A small peak at 400 nm in the transmission spectra is distinctive to the edge of fundamental absorption of the film. It shifts by 10–15 nm to the UV region after laser treatment and remains permanent irrespective to the influence regime.

The obtained optical characteristics were used to calculate the extinction and estimate the energy of the bandgap for indirect allowed transitions. The action of laser radiation led to an increase in the bandgap of the film from 3.27 eV to 3.32 - 3.36 eV (Fig. 10), so-called blue shift. This shift associated with an increase in the concentration of free electrons in the material. After generation, new charge carriers fill the lower levels of the conduction band of the AZO:Ag film. That leads to the fact that electrons from the semiconductor valence band need to spend more energy to overcome the bandgap, which requires the action of photons with a shorter wavelength. An increase in the concentration of free electrons is associated with laser activation of Al ions, as well as with an increase of oxygen vacancies in the AZO matrix, which are electron donors [7]. Moreover, Ag NPs were additional sources of charge carriers. Ag electrons under the irradiation could move to the AZO conduction band.

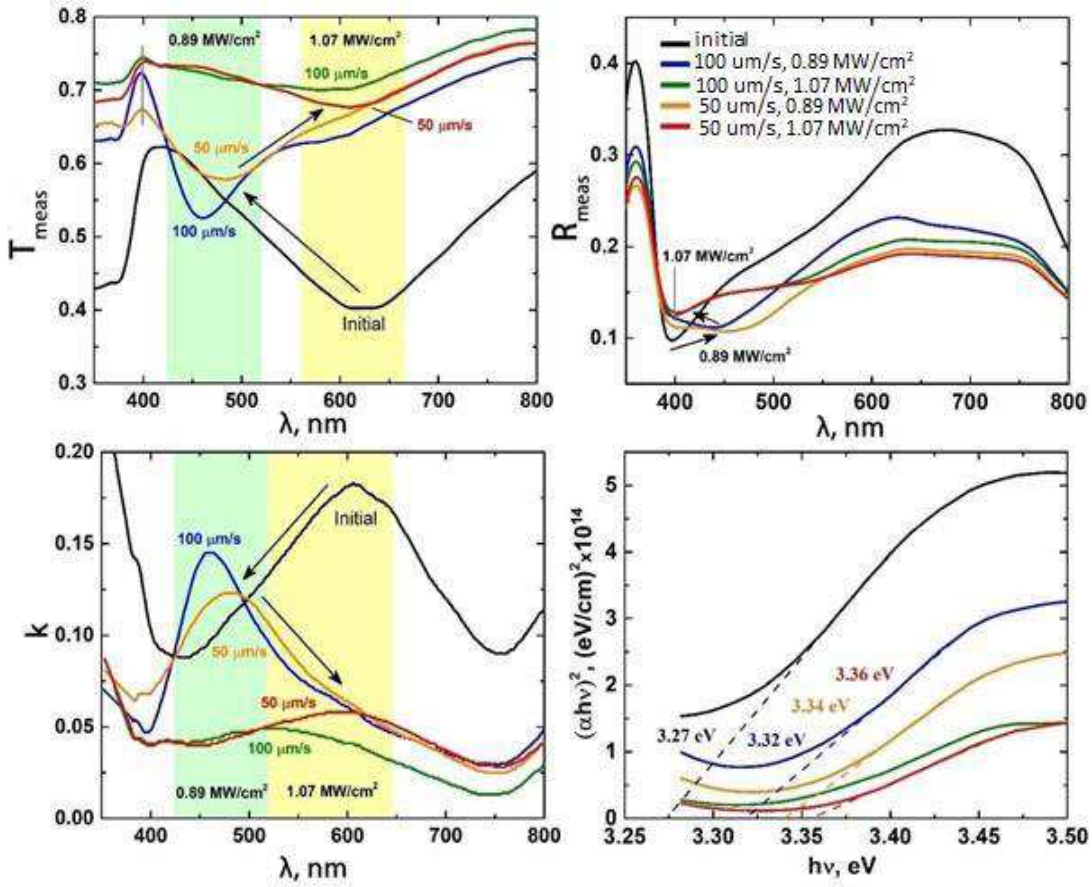

Fig. 10. Transmission, reflection, extinction, and curve $(\alpha h\nu)^2$ for the original film (black) and recorded tracks 100 μm/s, 0.89 MW/cm^2 (blue); 100 μm/s, 1.07 MW/cm^2 (green); 50 μm/s, 0.89 MW/cm^2 (orange); 50 μm/s, 1.07 MW/cm^2 (red).

3.3 Photothermal structure modification

The mechanism of laser modification of the film is associated with thermal processes caused by the action of the heat source on the film matrix and NPs. The formation of the heat source in the laser beam focusing area is associated with the partial absorption of radiation on the matrix and NPs. The substrate under the film did not absorb laser radiation but was heated due to heat transfer from the heated film. In the laser radiation absorption area, an abrupt heating of the material occurred. With a temperature of 640 – 776 °C (913 – 1049 K) at the epicenter and a heat source size of 3 – 6 μm, the temperature gradient dT/dr reached 192 – 213 °C/μm. The heating rate was (8 – 26) $*10^3$ °C/s when the laser spot moved at a velocity of 50 – 100 μm/s. Heating from room temperature to the maximum temperature proceeded in 0.5 – 1.0 s. That led to extreme conditions for heating the film with various stages of its modification. All data of the heat source was difficult to measure in the experiment, so it was modeled based on the obtained information about the modified regions and thermophysical characteristics of the film (see supplementary).

In the beginning of laser treatment Ag NPs decomposed into atoms, ions, and monomers. They concentrated at the boundaries of AZO crystals (Fig. N, I). Next, there was a diffusion mass transfer of Ag in the form of monomers along the temperature gradient from the center of the film to its surface and to the film-substrate interface, where the temperature was lower (Fig. N, II). Simultaneously with the mass transfer of Ag, the AZO matrix thermally compacted and recrystallized. Assumably, at this moment the absorption capacity of the film decreased due to the destruction of large Ag NPs. After that, the heat front began to spread outside the film, that led to the softening of the substrate under the exposed area due to heat transfer from the heated film to the glass substrate. Due to this phenomenon, the outflow of Ag monomers from the film to the substrate sharply increased. When the heat source was removed, Ag nanoclusters grew on the film surface during its cooling (Fig. N, III). In the softened substrate Ag monomers began to agglomerate forming Ag NPs under the film (Fig. N, IV). The growth of Ag NPs in the substrate ended only when the heat source was removed, the temperature dropped, and the glass solidified. Since the film modification was occurred due to thermal action of laser radiation, such mechanism can be called photothermal.

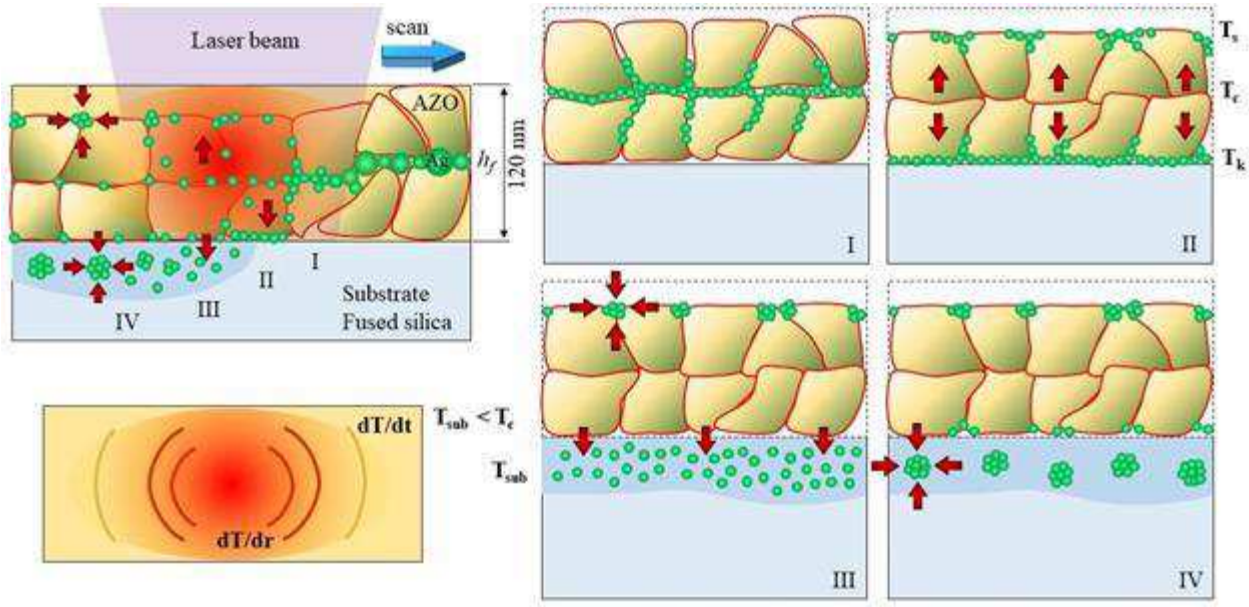

Fig. 11. The scheme of AZO:Ag film photothermal modification with the following stages: I. Decomposition of Ag NPs into monomers; II. mass transfer of Ag monomers from the center of the film to the surface and to the film-substrate interface; III. the outflow of Ag monomers from the film to the substrate during its softening, as well as the growth of Ag nanoclusters on the film surface; IV. agglomeration of Ag monomers and growth of NPs in the substrate.

4. Conclusion

Under the influence of CW radiation with a wavelength of 405 nm, the structure of AlZnO films with silver nanoparticles on a glass substrate was recrystallized, similar to the pulsed laser recrystallization with excimer lasers. The main difference was that the laser radiation used had a quantum energy below bandgap. The treatment was possible due to the presence of silver nanoparticles, which increased the absorption efficiency. As a result of recrystallization, smaller crystallites were combined into larger ones, about 80 nm in size. Initial nanoparticles with diameters of about 65 nm were concentrated within individual crystallites after laser treatment, the particle diameter decreased to 10 nm or less. At 0.89 MW/cm^2 at both scan rates, the maximum of the plasmon resonance peak in the transmission and extinction spectra was shifted to a wavelength of 450 nm; at 1.07 MW/cm^2, a significant decrease in the peak intensity was obtained. The study of the bandgap showed that it increased from 3.27 eV to 3.36 eV due to an increase in the concentration of charge carriers after exposure. A photothermal mechanism for film modification was proposed, the recrystallization of AZO and a decrease in the size of nanoparticles occurred due to the thermal effect of laser radiation.

Supplementary

To estimate the range and gradient of film temperatures in the region of laser action, as well as the heating rate, the heat source was modeled. In the region of a laser spot with a rectangular cross section, the laser radiation was partially absorbed, and a heat source was formed. To describe the heat source, a model of heating by CW laser radiation in the scanning mode was used [23]. The following approximations were used:

1. Laser radiation was absorbed only by the film and was not absorbed by the substrate, the transmission of the film at a wavelength of 405 nm (see fig. 2) changed from $T_{AZO} = 0.705$ to $T_{AZO:\,Ag} = 0.663$, and the reflection from $R_{AZO} = 0.022$ to $R_{AZO:\,Ag} = 0.008$, therefore, its absorption capacity was $A_{AZO} = 0.273$ and $A_{AZO:\,Ag} = 0.329$.
2. During the treatment, NPs were destroyed, which led to a decrease in the absorption of the film from $A_{AZO:\,Ag}$ to A_{AZO}. A depended on the time of thermal action τ in the XY plane as follows:

$$A(\tau,x,y) = A_{AZO:Ag}\left[1-0.085\exp\left(-4\frac{y^2}{y_0^2}\right)erfc\left(2\frac{x}{y_0}+\frac{\upsilon r_{hs}}{4a_f}\tau\right)\right], \quad (1)$$

$$\tau = \frac{1}{0.52r_{hs}}\sqrt{a_f\frac{2r_{hs}}{\upsilon}}, \quad (2)$$

there $2y_0$ – cross-sectional dimension of the modified track, a_f = 1.92 mm^2/s – thermal diffusivity of the film, υ = 100, 50 μm/s – scanning velocity, r_{hs} = 0.85 μm laser spot radius. For q = 0.89 MW/cm^2 y_0 = 0.9 μm, for q = 1.07 MW/cm^2 y_0 = 1.5 μm.

3. Laser spot shape corresponded to a square with a side $2r_{hs}$ = 1.7 μm.
4. Heat outflow from the heated area occurred into the air and into the substrate (fused silica) at the following thermal diffusivity values: a_{air} = 0.2107 mm^2/s and a_{sub} = 0.5956 mm^2/s.
5. Heat transfer at the film-air and film-substrate boundaries was determined by the following coefficients: $\alpha_{FA} = 25.15$ W/m^{2}K and $\alpha_{FS} = 100.9$ W/m^{2}K.
6. Thermal conductivity, heat capacity, and density of the film during laser exposure were constant.

Absorbed energy flux was set by the following equations for the environment, the film, and the substrate below it:

$$Q(z) = \begin{cases} \alpha_{FA}\left(T_{\max}-T_0\right)\pi r_{hs}^2, & z < -0.5h_f, \\ \dfrac{A(\tau_s,x,y)P-\left(\alpha_{FA}+\alpha_{FS}\right)\left(T_{\max}-T_0\right)\pi r_{hs}^2}{128kR}, & z \le 0.5h_f \wedge z \ge -0.5h_f,, \\ \alpha_{FS}\left(T_{\max}-T_0\right)\pi r_{hs}^2, & z < 0.5h_f, \end{cases} \quad (3)$$

there h_f – film thickness, T_0 = 273 K, T_{max} – maximum temperature, k = 5.4 W/mK – thermal conductivity, P = 20 and 24 mW – incident power. Radius R is the average size of the heat source, equal to

$$R = \sqrt[3]{r_{hs}^2 h_f} \,. \tag{4}$$

The temperature distribution in the affected area was described as the heat inflow and outflow:

$$\begin{bmatrix} dT_x(x,\tau) \\ dT_y(y,\tau) \\ dT_z(z,\tau) \end{bmatrix} = \begin{bmatrix} erfc\left(\frac{x-r_{hs}}{R\tau}+\frac{\upsilon R}{4a}\tau\right)-erfc\left(\frac{x+r_{hs}}{R\tau}+\frac{\upsilon R}{4a}\tau\right) \\ erfc\left(\frac{y-r_{hs}}{R\tau}\right)-erfc\left(\frac{y+r_{hs}}{R\tau}\right) \\ erfc\left(\frac{z-0.5h_f}{R\tau}\right)-erfc\left(\frac{z+0.5h_f}{R\tau}\right) \end{bmatrix}, \tag{5}$$

there a – thermal diffusivity of air (a_{air}), film (a_f), and substrate (a_{sub}):

$$a = \begin{cases} a_{air}, & z < -0.5h_f, \\ a_f, & z \le 0.5h_f \wedge z \ge -0.5h_f, \\ a_{sub}, & z < 0.5h_f. \end{cases} \tag{6}$$

Temperature distribution:

$$T(x,y,z) = Q(z)\int_0^t dT_x(x,\tau)\,dT_y(y,\tau)\,dT_z(z,\tau)\,\tau d\tau, \tag{7}$$

there t – effective heating time of the film $t = R^{-1}(2ar_{hs}/\upsilon)^{0.5}$.

Maximum temperatures and the heat source shape in the laser action zone were estimated (fig. 01). After reaching the maximum temperature, the absorption capacity of the film dropped. This led to a decrease in temperature already at the center of the laser spot. The maximum temperature at the center of the laser spot could reach 640–776 °C (913 – 1049 K), with heating rate (8 – 26) *10^3 °C/s. Due to the small size of the laser spot, the temperature gradient could reach values 192 – 213 °C/ μm. Such small size of the laser spot and the localization of the heat source ensured high heating temperatures at low radiation power, sufficient for melting the matrix and modifying NPs in it.

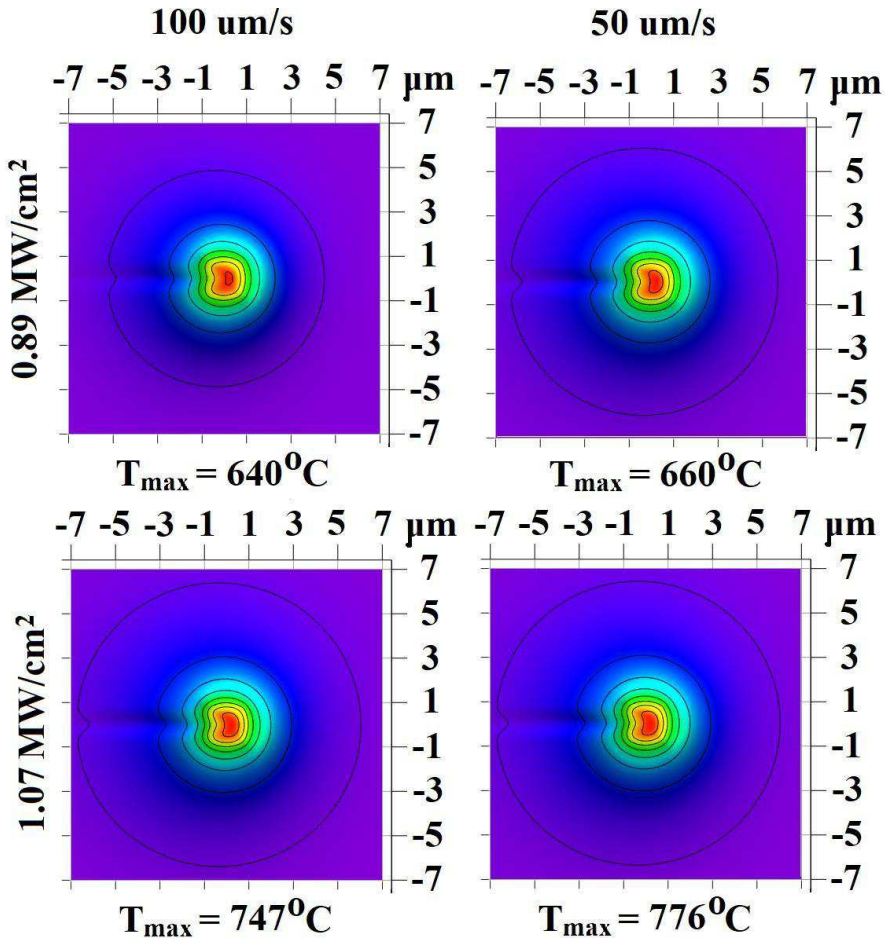

Fig. 01. shape of the heat source depending on the radiation intensity and scanning velocity.

Funding

This research was funded by the grant of Russian Science Foundation (project No. 19-79-10208).

Acknowledgments

SEM measurements were done on the base of Interdisciplinary Resource Centre for Nanotechnology, Research Park, St. Petersburg State University.

Declaration of Competing Interest

The authors declare that they have no known competing financial interests or personal relationships that could have appeared to influence the work reported in this paper.

CRediT authorship contribution statement

Maksim M. Sergeev: Conceptualization, Methodology, Writing - Original Draft, Funding acquisition, Supervision. **Vladislav R. Gresko:** Investigation, Visualization, Validation, Writing - Original Draft. **Yaroslava M. Andreeva:** Writing - Review & Editing, Validation. **Lilia A. Sokura:** Resources. **Elena V. Shirshneva-Vaschenko:** Resources. **Tatiana E. Itina:** Writing - Review & Editing, Validation. **Georgy V. Varigyn:** Investigation.

References

[1] Rwenyagila ER, Agyei-Tuffour B, Zebaze Kana MG, Akin-Ojo O, Soboyejo WO. Optical properties of ZnO/Al/ZnO multilayer films for large area transparent electrodes. Journal of Materials Research 2014;29. https://doi.org/10.1557/jmr.2014.298.

[2] Islam MM, Ishizuka S, Yamada A, Matsubara K, Niki S, Sakurai T, et al. Thickness study of Al:ZnO film for application as a window layer in Cu(In 1-x Ga x)Se 2 thin film solar cell. Applied Surface Science 2011;257. https://doi.org/10.1016/j.apsusc.2010.11.169.

[3] Singh S, Park SH. Fabrication and characterization of Al:ZnO based MSM ultraviolet photodetectors. Superlattices and Microstructures 2015;86. https://doi.org/10.1016/j.spmi.2015.08.019.

[4] Zhang MY, Cheng GJ. Highly conductive and transparent alumina-doped ZnO films processed by direct pulsed laser recrystallization at room temperature. Applied Physics Letters 2011;99. https://doi.org/10.1063/1.3622645.

[5] Mass J, Bhattacharya P, Katiyar RS. Effect of high substrate temperature on Al-doped ZnO thin films grown by pulsed laser deposition. Materials Science and Engineering B: Solid-State Materials for Advanced Technology 2003;103. https://doi.org/10.1016/S0921-5107(03)00127-2.

[6] Ning ZY, Cheng SH, Ge SB, Chao Y, Gang ZQ, Zhang YX, et al. Preparation and characterization of ZnO: Al films by pulsed laser deposition. Thin Solid Films 1997;307. https://doi.org/10.1016/S0040-6090(97)00303-9.

[7] Nian Q, Callahan M, Saei M, Look D, Efstathiadis H, Bailey J, et al. Large scale laser crystallization of solution-based alumina-doped zinc oxide (AZO) Nanoinks for highly transparent conductive electrode. Scientific Reports 2015;5. https://doi.org/10.1038/srep15517.

[8] Hagendorfer H, Lienau K, Nishiwaki S, Fella CM, Kranz L, Uhl AR, et al. Highly transparent and conductive ZnO: Al thin films from a low temperature aqueous solution approach. Advanced Materials 2014;26. https://doi.org/10.1002/adma.201303186.

[9] Nian Q, Zhang MY, Schwartz BD, Cheng GJ. Ultraviolet laser crystallized ZnO:Al films on sapphire with high Hall mobility for simultaneous enhancement of conductivity and transparency. Applied Physics Letters 2014;104. https://doi.org/10.1063/1.4879643.

[10] Chou YH, Hong K bin, Chung YC, Chang CT, Chou BT, Lin TR, et al. Metal for Plasmonic Ultraviolet Laser: Al or Ag? IEEE Journal of Selected Topics in Quantum Electronics 2017;23. https://doi.org/10.1109/JSTQE.2017.2748521.

[11] Sokura LA, Shirshneva-Vaschenko E v., Kirilenko DA, Snezhnaia ZG, Shirshnev PS, Romanov AE. Electron-microscopy study of ordered silver nanoparticles synthesized in a ZnO:Al polycrystalline film. Journal of Physics: Conference Series, vol. 1410, 2019. https://doi.org/10.1088/1742-6596/1410/1/012170.

[12] van Cuong G, Trung T, Tue NA, Tuan NA. Cobalt content- and magnetic field-dependent transmission behaviors of red laser light for Co[sbnd]Al2O3 granular thin films. Optical Materials 2017;69. https://doi.org/10.1016/j.optmat.2017.04.042.

[13] Nasser H, Saleh ZM, Özkol E, Günoven M, Bek A, Turan R. Fabrication of Ag Nanoparticles Embedded in Al:ZnO as Potential Light-Trapping Plasmonic Interface for Thin Film Solar Cells. Plasmonics 2013;8. https://doi.org/10.1007/s11468-013-9562-6.

[14] Karimi-Maleh H, Kumar BG, Rajendran S, Qin J, Vadivel S, Durgalakshmi D, et al. Tuning of metal oxides photocatalytic performance using Ag nanoparticles integration. Journal of Molecular Liquids 2020;314. https://doi.org/10.1016/j.molliq.2020.113588.

[15] Tzeng S-K, Hon M-H, Leu I-C. Improving the Performance of a Zinc Oxide Nanowire Ultraviolet Photodetector by Adding Silver Nanoparticles. Journal of The Electrochemical Society 2012;159. https://doi.org/10.1149/2.088204jes.

[16] Shirshneva-Vaschenko E v., Sokura LA, Shirshnev PS, Kirilenko DA, Snezhnaia ZG, Bauman DA, et al. Preparation of transparent N-ZnO:Al / p-CuAlCrO 2 heterojunction diode by sol-gel technology. Reviews on Advanced Materials Science 2018;57. https://doi.org/10.1515/rams-2018-0061.

[17] Al-Ghamdi AA, Al-Hartomy OA, el Okr M, Nawar AM, El-Gazzar S, El-Tantawy F, et al. Semiconducting properties of Al doped ZnO thin films. Spectrochimica Acta - Part A: Molecular and Biomolecular Spectroscopy 2014;131. https://doi.org/10.1016/j.saa.2014.04.020.

[18] Xue SW, Zu XT, Zheng WG, Deng HX, Xiang X. Effects of Al doping concentration on optical parameters of ZnO:Al thin films by sol-gel technique. Physica B: Condensed Matter 2006;381. https://doi.org/10.1016/j.physb.2006.01.342.

[19] Caglar M, Ilican S, Caglar Y, Yakuphanoglu F. The effects of Al doping on the optical constants of ZnO thin films prepared by spray pyrolysis method. Journal of Materials Science: Materials in Electronics, vol. 19, 2008. https://doi.org/10.1007/s10854-007-9386-2.

[20] Tomlin SG. Optical reflection and transmission formulae for thin films. Journal of Physics D: Applied Physics 1968;1. https://doi.org/10.1088/0022-3727/1/12/312.

[21] Abutalib MM, Rajeh A. Influence of ZnO/Ag nanoparticles doping on the structural, thermal, optical and electrical properties of PAM/PEO composite. Physica B: Condensed Matter 2020;578. https://doi.org/10.1016/j.physb.2019.411796.

[22] Aziz SB, Brza MA, Nofal MM, Abdulwahid RT, Hussen SA, Hussein AM, et al. A comprehensive review on optical properties of polymer electrolytes and composites. Materials 2020;13. https://doi.org/10.3390/MA13173675.

[23] Miyamoto I, Horn A, Gottmann J. Local melting of glass material and its application to direct fusion welding by Ps-laser pulses. Journal of Laser Micro Nanoengineering 2007;2. https://doi.org/10.2961/jlmn.2007.01.0002.